Report on GISMO Run #2

Updated May 2009

J. Staguhn, R. Arendt, D. Benford, D. Fixsen, S. Maher & E. Sharp

Summary

Performance: The GISMO instrument was assembled in the IRAM 30m telescope's main building lab and then installed on the telescope on Pico Veleta, Spain, for observations beginning Tuesday, October 21, 2008. In order to provide observing capabilities under all weather conditions we used a quartz 40% transmission neutral density filter at 4 K. During mostly mediocre weather condition we typically achieved sensitivities in our maps that correspond to between 40 and 50 mJy/sqrt(s) for the equivalent integration time of all pixels that were flagged as good. These values are consistent with our refined atmospheric efficiency model calculations that predict NEFDs ranging from 28 to 56 mJy/sqrt(s) for GISMO's optical configuration and observing conditions ranging between 10% and 40% line of sight opacities. The noise in our coadded maps (with few thousand seconds of integration time) scales very well with the square root of time.

Due to a short in one of the four SQUID multiplexers we had to turn off the readout of one of our quadrants in the array. Typically 20% to 25% of the remaining detector pixels were not working or showed excess noise and therefore had to be flagged as bad. A problem with one of the detector box connectors was likely causing most of the observed excess noise. With the resulting pixel efficiency of about 50% we obtained a small map rms of typically1 mJy in one hour of integration time in relatively bad weather.

Expectations for future performance: By now we have replaced the bad SQUID multiplexer, as well as the bad connector. As a result we observe virtually no excess noise in any of the pixels and have now a total pixel yield of more than 90%. Our simulations indicate that we will gain a factor of 2.4 in observing efficiency if we take out the neutral density filter, which we plan to do during good to average weather conditions. With a good pixel yield of 90% we can expect to achieve the same observing efficiency we obtained in run 2 in less than a quarter of the integration time. Under typical conditions (20% line of sight sky opacity) we expect to achieve a good pixel map sensitivity of 22 mJy/sqrt(s) or a map NEFD of 1mJy in an observation lasting about 8 minutes. With the right observing strategy for point sources of known position, this sensitivity theoretically can further be reduced by a factor of 1.5 (2.3 in observing time).

Instrument Configuration for Run #2

A number of modifications were implemented in the GISMO instrument to improve on the configuration used during the first observing run in November, 2007. In particular, the two major problems encountered during that run were fixed: the stray light problem arising from undersized baffles, and the mechanical design of the detector package which led to the detachment of one ceramic board that holds cryogenic readout chips. The detachment had resulted in the loss of the ability to read out one quadrant of the detector array during the first observing run. We had to replace the SQUID multiplexer chip

together with its shunt resistor and Nyquist chip from that quadrant. The circuit board in the detector package was completely re-designed to prevent a repeat of this problem, and the new board allowed us to use a more reliable commercially-made cold harness.

As in observing run #1, we were still using a 40% transmission neutral density filter in the instrument. This was done to ensure that the detectors would not saturate under any observing conditions. Since then, however, we have identified a ground loop problem that appears to have resulted in extra electrical power dissipation in the detectors or in the SQUID mux chip, that might have heated up the array. Our current lab tests after fixing this problem indicate that the radiative load margin for our detectors has been improved, so we anticipate that under good to normal conditions there will be no need to use this filter. We are currently designing a warm neutral density filter, based on a polarizing grid with the intent to allow GISMO observations also under worse than normal weather conditions without having to warmup the instrument. We are also exploring the use of two cold neutral density filters that can be moved into and out of the beam. The latter would be our preferred solution since it would effectively increase the dynamic range of the detectors with almost no impact on the noise performance under almost all observing conditions. We will later in this document discuss the expected improvement of the signal to noise performance of the instrument without use of a neutral density filter.

During the observing run we identified a problem with the replacement SQUID multiplexer chip we had installed into the package after the mechanical failure during run #1. An internal short in the chip itself caused a crosstalk of the first stage SQUID feedback of quadrant 1 into the second stage feedback of quadrants 2 & 3. The resulting crosstalk from quadrant 1 into 2 and 3 was significant, and therefore we decided to conduct all observations during run #2 with quadrant 1 disabled. The yield of working detectors in the other quadrants was around 80%, however, a few of those pixels were at times up to a factor of 2 noisier than usual, and therefore often were flagged as bad during data analysis. As a result, a typical pixel yield for a given observation turned out to be about 50% (which includes the quadrant we could not turn on). The increased noise in some of the detectors was likely the result of an address line short that we had introduced with a last-minute replacement of a connector. This problem has since been fixed, and we see a positive effect in terms of the detector stability and apparent saturation power of the detectors. We are currently in the process of quantifying this. As presently operated in our lab, we measure a total good pixel yield of 90% or more. This number will be lower for higher sky power without the use of the neutral density filter (due to variations in the saturation power of the detectors).

Mitigation of discrete frequency spikes in the observed power spectra:

For the second observing run we completely opto-decoupled all electrical signal lines going into and out of the dewar. We also wrapped the dewar stand with eccosorb sheets and the local oscillators in the receiver cabin were turned off by IRAM staff. As a result, we saw significantly fewer and lower amplitudes of discrete spikes in our detector current noise density spectra than in the first observing run. The detector noise spectra we obtained in the receiver cabin with the dewar window closed are very clean, and similar to what we observed in the lab at GSFC. In the out-of-signal band only the 50/60 Hz spike contains appreciable power (Figure 1). The physical units of pA/√Hz shown in the figure are derived from two independent methods: one which requires the knowledge of the bias shunt resistor value and another, the statistical analysis of flux quantum jumps, which does not require any knowledge about passive elements in the circuit). Few prominent lines can be seen, such as one at 11 Hz, which were measured as vibrations present in the receiver cabin by reading out the accelerometers of an iPhone. The observed noise density at frequencies ≳3 Hz are highly consistent with the expected fundamentally limited noise levels (Staguhn et al. 2006, *NIMPR-A*, v.559, pp. 545-547; *"Characterization of TES bolometers used in 2-dimensional Backshort-Under-Grid (BUG) arrays for far-infrared astronomy"*).

Beam spillover issues observed during run #1:

The hot spillover observed during run #1 was not present on run #2. This is a result of the

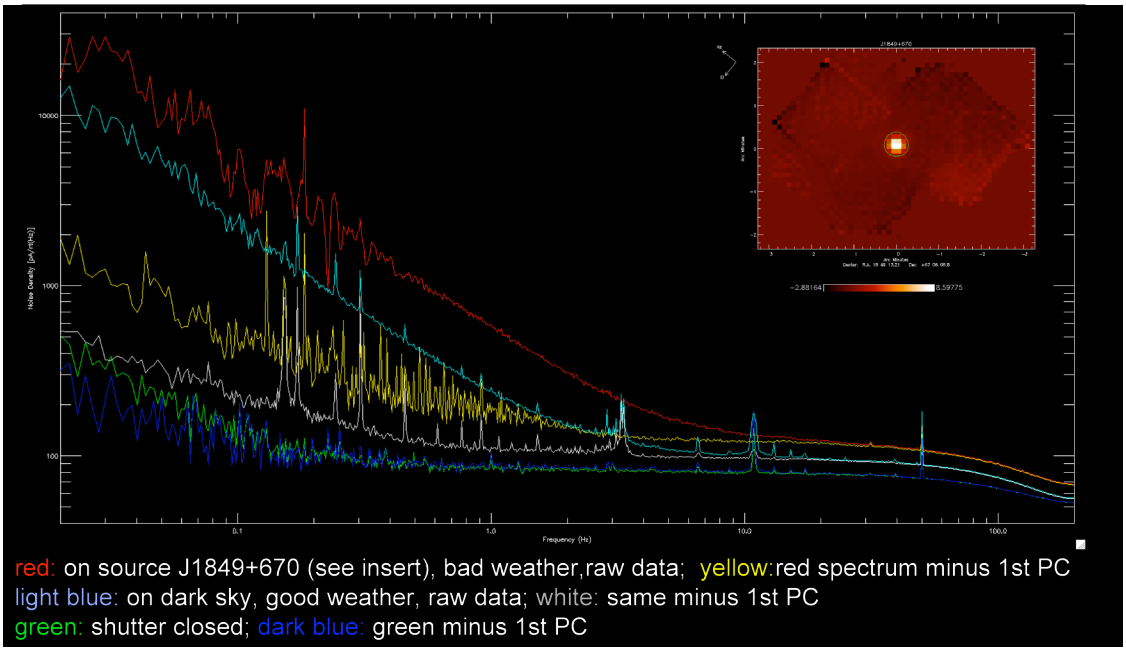

Figure 1: Current noise density spectrum measured for 64 GISMO pixels on the sky under different weather conditions and with the shutter closed as indicated on the labels. Note the quasar's signal in the Lissajous signal band between 0.1 and 1.5 Hz in the yellow spectrum.

redesign of GISMO's cold baffles, by taking into account a more precise determination of the beam size and shape (which is not exactly circular) at each baffle location. The spillover had forced us during run #1 to restrict the GISMO dewar window size, reducing the overall system efficiency. During run #2, the full illuminated aperture was available.

Instrument setup issues:

During the setup on the telescope, we detected a problem with the isolated optical bench on which instruments are mounted. It turned out that the pistons for the air pressure control were defective and had been deactivated by the IRAM staff. Therefore, there was no pneumatic isolation for the optical bench in the first one and a half days of the run, which resulted in vibrations propagating through to our dewar that produced increased noise. On the following day, the bench was pressurized again and the noise spectra were significantly better than seen in run #1 (see Fig. 1 which shows data with the bench pressurized). However, the optical bench would often oscillate so that the instrument stand occasionally bumped into a metal structure in the receiver cabin. The IRAM staff therefore glued a piece of rubber as "bumper" to the metal structure. As a consequence, occasionally we see broad spikes in our data at the frequency of the azimuth movement of the telescope, corresponding to each bumping event. In those cases we apply a notch filter at that frequency to our data. However, since these spikes are non-stationary it is impossible to completely remove them from the data.

Observing modes:

The data during run #1 were observed in on-the-fly mode, which is a slow regular rectangular grid rastering, both with and without the secondary wobbling. In run #2, we used Lissajous scans with fixed secondary position. Lissajous scans produce faster crossing times and enable greater cross-linking of observations, thereby reducing the effects of atmospheric and system drift contributions. Another advantage is that the fundamental telescope frequencies are not coinciding with signal crossing times.

Results from observations:

During run #2, we encountered worse weather conditions than in the 2007 observing run. This manifested itself most prominently in the fact that the sky noise (arising from temporal variations in the water vapor in the line of sight) had a higher frequency 1/f knee in the observed run #2 weather (see Fig. 1) than was observed under the very good conditions during run #1. Despite the fact that the bad weather did not allow us to demonstrate integrations well below sub-mJy levels, we were able obtain a significant number of astronomical observations that are now in the pipeline for publication. Examples follow below. Furthermore, the data enabled us to investigate the properties of the atmosphere under poor conditions and to test the ability of our data reduction algorithms for astronomical observations taken under these conditions. Figure 1 shows the total sky noise (red) and correlation-removed sky noise (yellow), both of which are still significantly above the noise floor provided by the GISMO instrument (green/blue) at frequencies higher > 10 Hz; at lower frequencies the sky 1/f noise becomes even more

prominent. In the case of bad weather, the noise is increased by more than sqrt(2), which – since the noise contributions add in quadrature - means the sky signal exceeds the phonon noise from the detector and the photon noise from the instrument itself. Under good weather conditions, however, the detector noise plus instrument internal photon noise is slightly higher than the white noise (≳1 Hz) from the sky. This is consistent with the noise models we present later in this report. Our simulations indicate, however, that once we remove the neutral density filter, we will be sky-noise-dominated under effectively all observing conditions.

Some reduced maps are presented in the following. Figures 2 and 3 show examples of maps produced using our quick reduction algorithms, which were generated right after the observations (and can be produced by an automated pipeline of processing). The quality of the maps demonstrates that we have adequate software tools to process observations in near-real time, and that the resulting images have few spurious features.

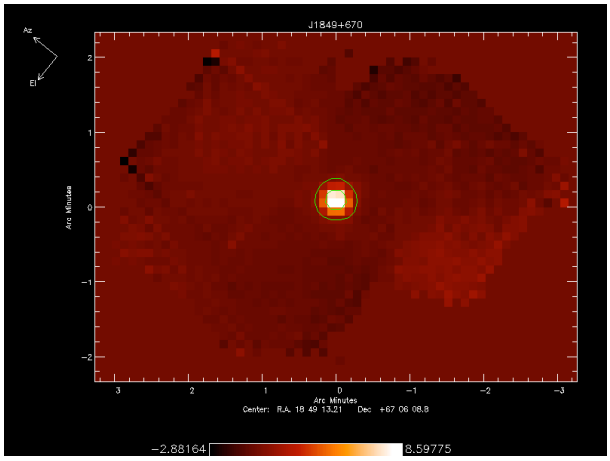

Figure 2: Image of J1849+670 from dataset shown in Fig. 1. A Gaussian fit yields a beam size of 15.8”x16.2”, close to the diffraction limited beamsize of 15”.

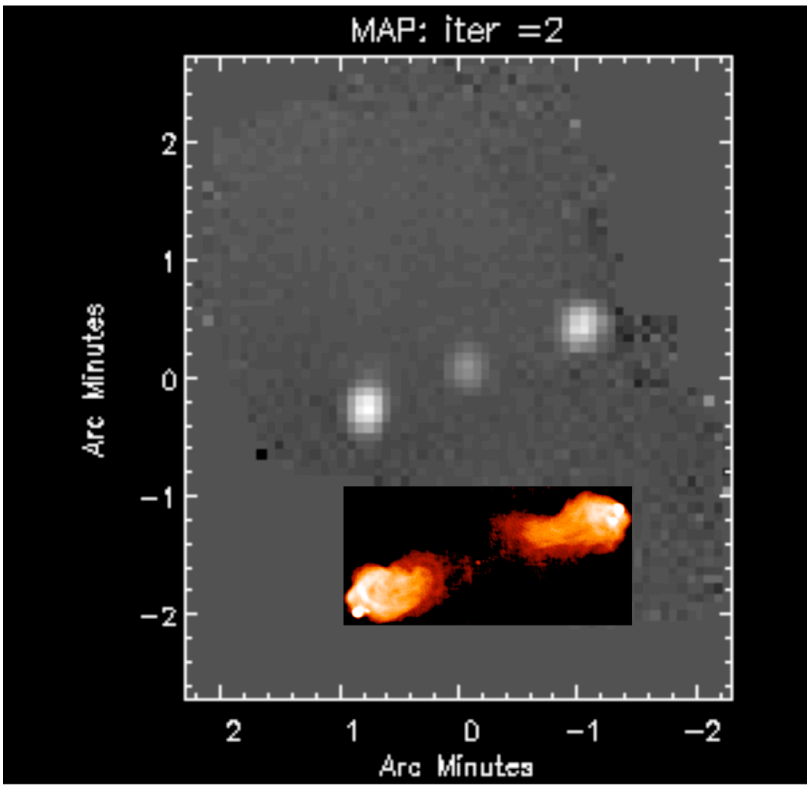

Figure 3: Composite picture showing the GISMO image of Cygnus A at 2mm (grey) and at the VLA image at 21 cm (inset).

The following two figures demonstrate our ability to successfully reduce extended sources using more advanced data reduction techniques. Figure 4 shows our observations of the supernova remnant Cas A. In the case of the dark cloud IRDC 30 (Figure 5, which features a scale for the measured flux in Jy/beam) we have clearly demonstrated that GISMO can detect dust emission in extended sources down to levels of <10 mJy/beam (the feature in the North-East, also seen in the MAMBO map, has a peak emission of 10 mJy/beam).

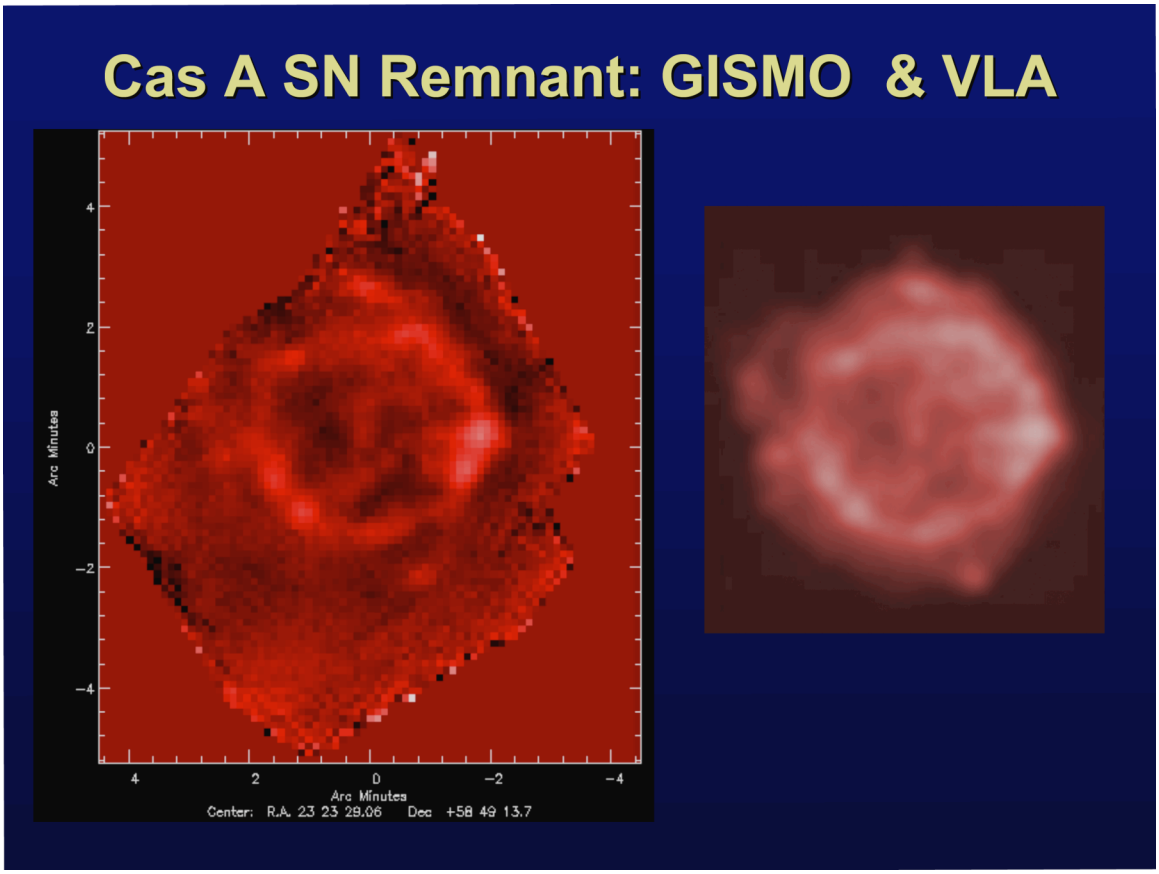

Figure 4: *left:* GISMO observations of the Cas A supernova remnant. *Right:* VLA 21 cm observations of Cas A, smoothed to GISMO's angular resolution.

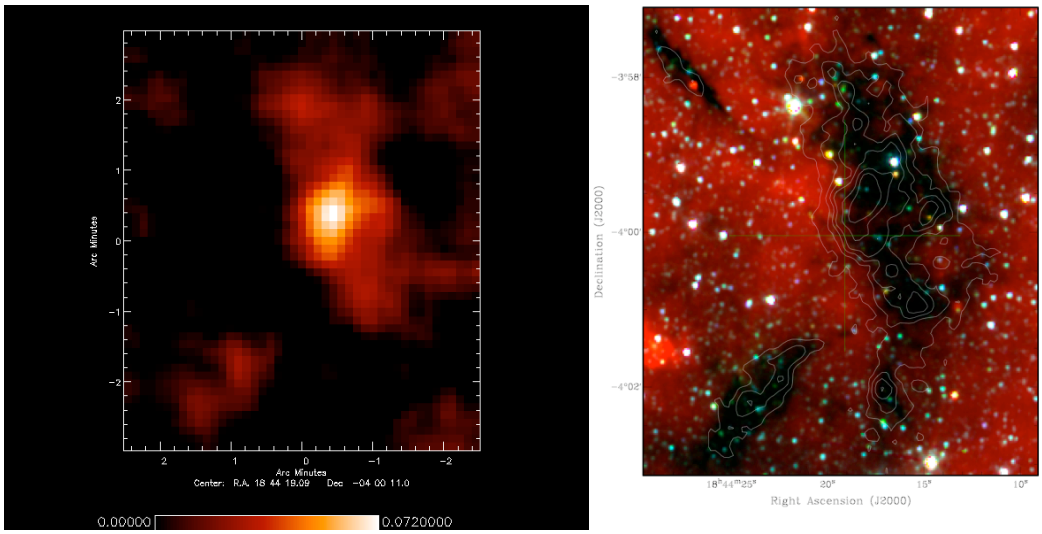

Figure 5: *left*: The Infrared Dark Cloud IRDC 30 observed with GISMO; *right:* 8μm image from IRAC (color) and MAMBO at 1.3 mm (contours). The flux in the GISMO map is shown in Jy/beam. Millimeter-wave emission is seen where absorption is highest in the IRAC image.

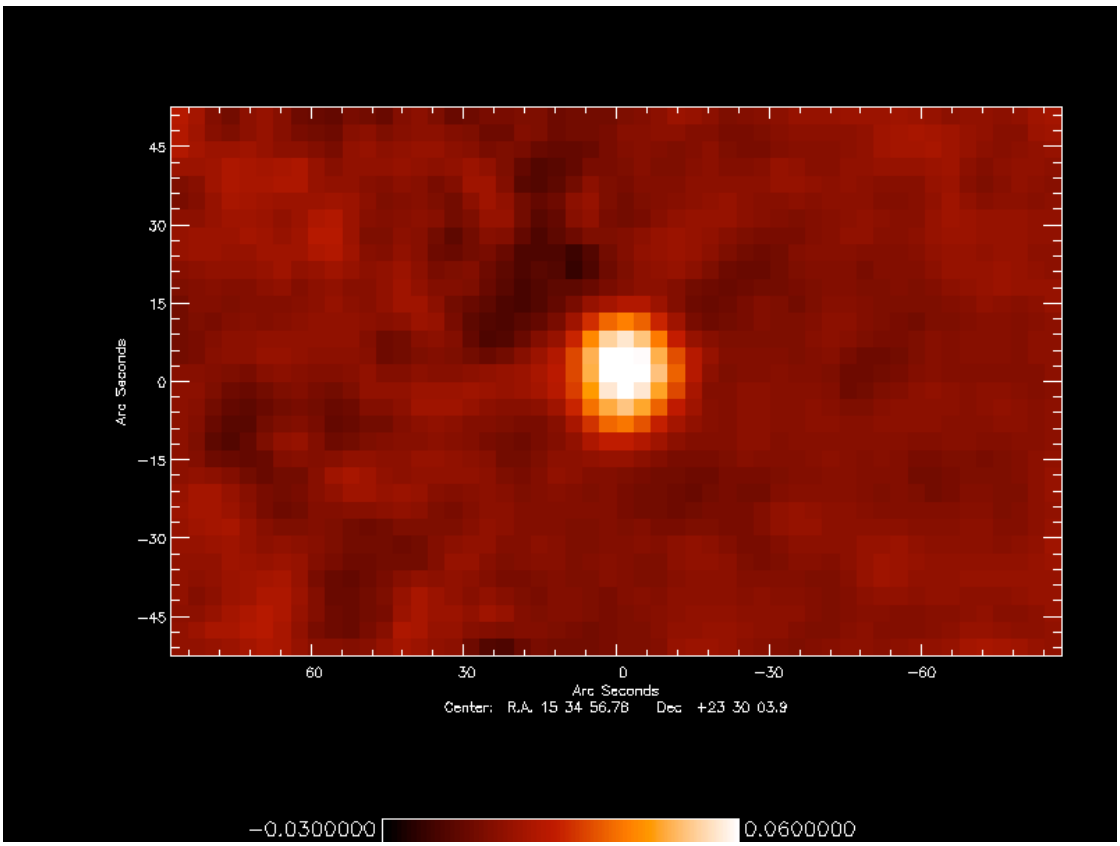

Figure 6: GISMO 2mm map of Arp220. The displayed units are Jy/beam. The measured flux of this ULIRG is (104 +/- 2) mJy. The quoted uncertainty does not include calibration uncertainties.

Figures 6 and 7 demonstrate GISMO's performance for point source observations. Figure 6 shows the high signal-to-noise GISMO map of the prototypical ULIRG Arp 220. We obtain a 2mm flux of (104 +/- 2) mJy. Note that the quoted uncertainty does not include calibration uncertainties. Figure 7 shows a section of our observed map of SDSS J1148+5251 around the presumed position of the source (the pointing offset in the map was determined from a quasar measurement right before these observations), which is at a redshift of z=6.42. The weather during the observations was quite unstable, including periods when the telescope was embedded in fog. The data clearly showed a peak at the azimuth Lissajous frequency, which we believe was caused by the GISMO optical stand hitting the rubber bumper described earlier in this report. After we applied a notch filter at that frequency to the data, the resulting maps showed significantly reduced large scale spurious structures. The rms noise in the map shown is 900 microJy. With an average pixel integration time of 2,500 seconds, this corresponds to a sensitivity of 45 mJy/rt(s), consistent with the predicted instrument performance in the weather conditions present during the observations (Fig.9). A discussion of the obtained vs. expected noise performance of the instrument follows in the next section. A Gaussian fit with fixed width corresponding to the instrument's beam size yields a value of (2 +/- 1) mJy/beam at the presumed position of the source. We characterize this fitted value as consistent with a non-detection, providing a 4σ upper limit of 3.6 mJy to the source flux. The expected

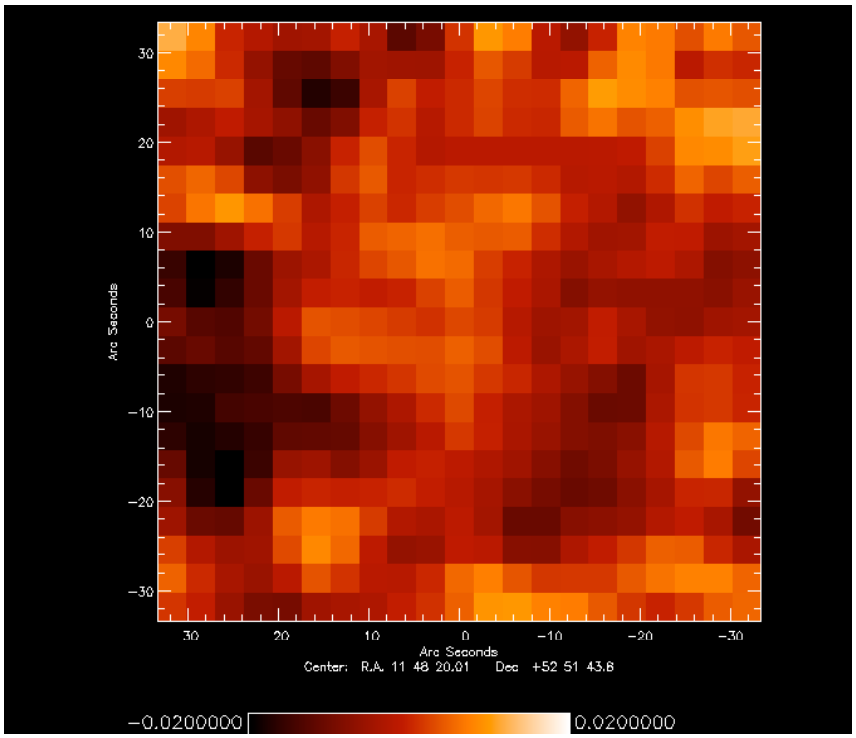

Figure 7: Area around the position of SDSS J1148+5251. The diffraction limited beam size is 16". The rms noise in the map is 900 microJy.

2mm flux of J1148+5251 is about 1.5 mJy, however, and so GISMO may well have detected this very distant quasar at low significance.

Instrument noise performance: In our preliminary report written at the end of observing run #2, we reported a significant discrepancy between the derived flux sensitivities of the instrument when different methods (see discussion below) were used to obtain signal-to-noise ratios from observations. Since then, a thorough analysis has reconciled these discrepancies and we are now able to derive consistent performance data for the instrument. Two major modifications of the assumptions we originally used, as well as improved data reduction algorithms, have led to these improvements in our understanding of the instrument: (1) we significantly improved our modeling of the optical performance of GISMO by incorporating measured filter transmission functions into our sensitivity calculations. (2) After studying the published values of QSO flux measurements (including variability around the period of late 2008), we had to revise the assumed 2mm flux of a number of the quasars that we had used to obtain a flux calibration factor (most planets are too bright for an accurate flux calibration, and the dimmer planets such as Uranus were only available for a few hours per night). Due to problems with our internal calibration system, we had to rely too heavily on those quasar calibrator measurements. In particular, we had trouble with both our internal calibration source and the window shutter mechanism, which had been intended to monitor the instrument gains at all times. IRAM also advised us not to rely on their tau meter readings to determine the atmospheric opacity. Indeed we only find a low correlation between the noise in our data and the tau meter readings, which varied widely over short

time periods. We have taken steps to ensure that our calibration scheme in future observing runs will work. The calibration method will involve improved versions of the internal calibration system with the addition of a total power calibration measurement technique (from detector I-V curves). This should provide a calibration that will be significantly more robust than it has been in the past.

Figs. 8, 9, 10 & 12 show the results from our atmospheric model calculations, which incorporate the 30m telescope plus GISMO optical parameters (in particular the GISMO filter functions and the 40% neutral density) for the range of weather conditions typical for the 30m site. The lower envelope of the plot displays the NEP expected for an atmospheric transmission of 90% at 150 GHz, which is the typical zenith transmission in winter conditions. The red line shows the expected summer zenith sky transmission of 80%, and the upper envelope is for the same summer conditions, but for 2 airmasses. Figure 8 demonstrates that – with the use of the 40% neutral density filter – the sky NEP ranges between $3 \cdot 10^{-17}$ and $6 \cdot 10^{-17}$ W/rt(Hz). The measured detector NEP is $4 \cdot 10^{-17}$ W/rt(Hz). Additionally we estimate that the photon noise from radiation inside the dewar contributes up to another $3 \cdot 10^{-17}$ W/rt(Hz). We therefore expect to observe a total NEP of between $6 \cdot 10^{-17}$ W/rt(Hz) and $8 \cdot 10^{-17}$ W/rt(Hz), depending on the weather. This means the measured NEP under good conditions can be up to a factor of 2 higher than that of the atmosphere only. Under moderate conditions the

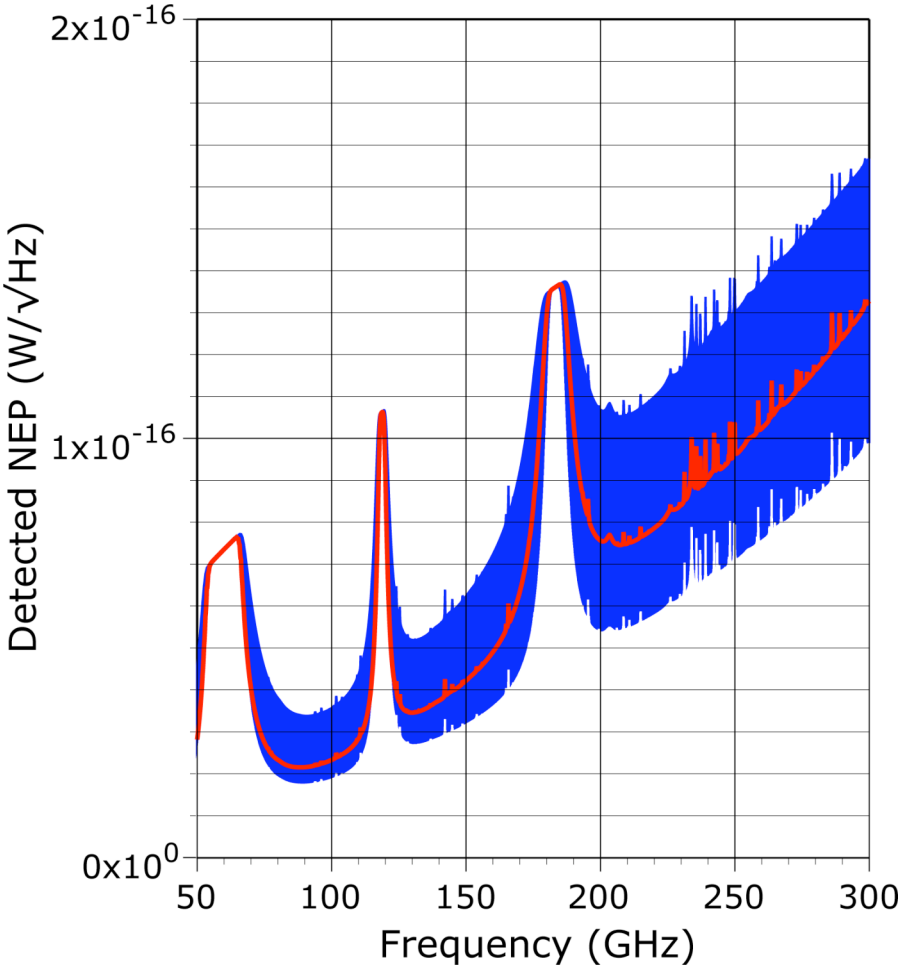

Figure 8: Detected Noise Equivalent Power (NEP) due to sky photons for 90% atmospheric transmission (bottom envelope), 80% transmission (red curve) and same conditions as shown in red line, but 2 airmasses (upper envelope), i.e. 60% transmission.

NEP is dominated by the atmosphere. The observed change in current noise densities with and without the dewar window open that are shown in Figure 1 are consistent with these values. Removing the neutral density filter in GISMO in the future, which we anticipate will be possible for excellent to normal observational conditions, will reduce the instrumental contribution to the NEP significantly and provide very near background limited performance of the instrument under even excellent atmospheric conditions. Figure 9 shows the expected NEFD for GISMO with the 40% transmission neutral density filter, whereas Fig. 10 shows the expected NEFD without the neutral density filter. A detailed document with our sky noise performance simulations, which includes calculations of GISMO's expected performance with and without the neutral density filter, is available.

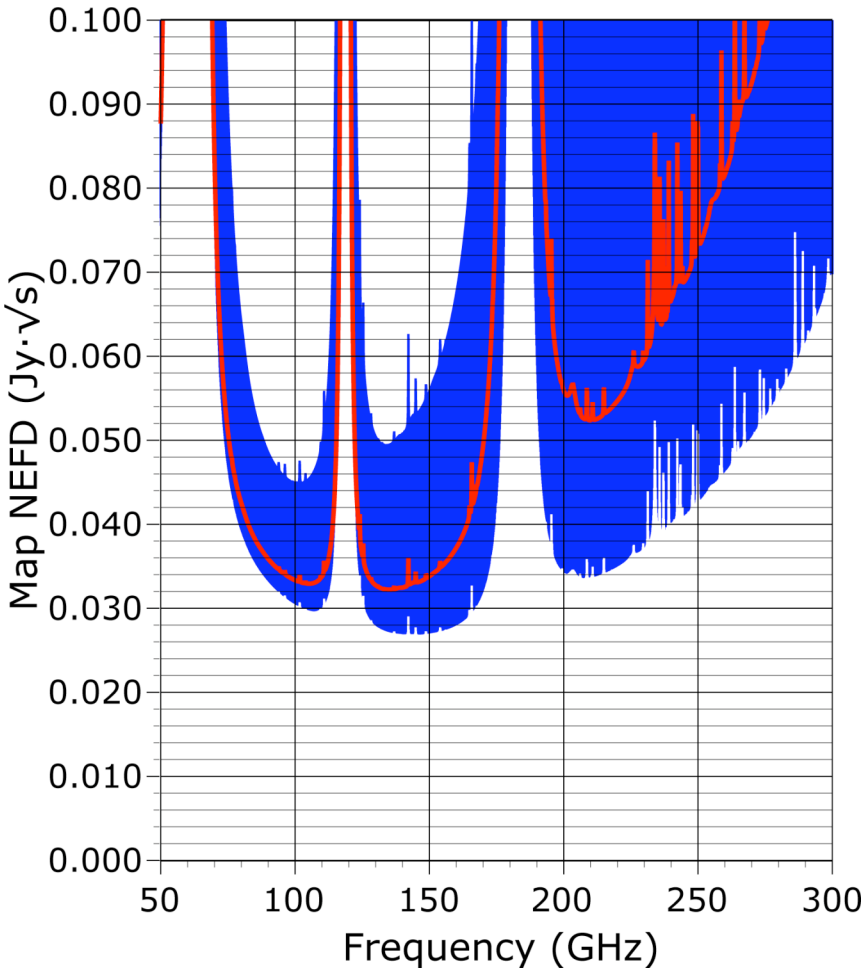

Figure 9: Total GISMO and IRAM 30m telescope Noise Equivalent Flux Density (NEFD) for point sources in typical weather ranging from good winter conditions (90% transmission) to normal summer conditions at 2 airmasses (60% transmission) **with** the 40% transmission neutral density filter used during run #2. The predicted range of the NEFD is between 27 and 56 mJy/rt(s) as would be measured from a processed map.

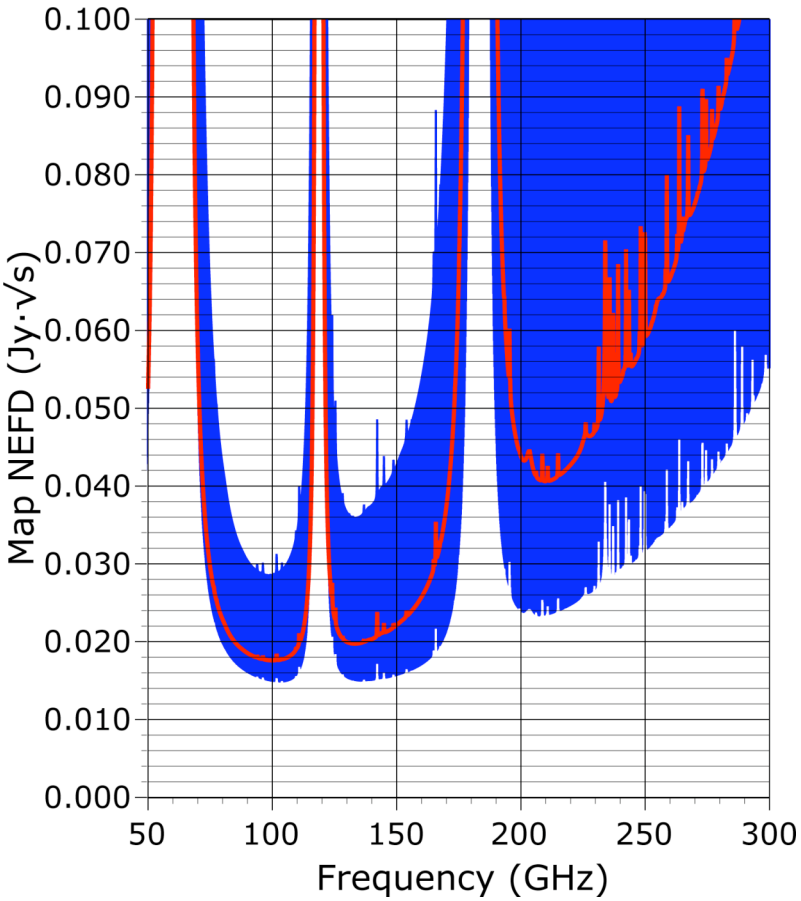

Figure 10: Total GISMO and IRAM 30m telescope Noise Equivalent Flux Density (NEFD) for point sources in typical weather ranging from good winter conditions (90% transmission) to normal summer conditions at 2 airmasses (60% transmission) **without** the 40% transmission neutral density filter used during run #2. The predicted range of the NEFD is between 16 and 44 mJy/rt(s) as would be measured from a processed map.

Instrument sensitivity derived from the data time stream:

In order to verify the noise performance of GISMO with a method that is independent of our map-making procedures, we investigated how the noise in our raw data stream compares to the signal we see from a known source. Figure 11 shows a section of the raw data of a single pixel, during which the quasar 3C545 crossed the pixel. The flux from 3C454 is assumed to be 12.5 Jy at 2mm. The corresponding noise fit is shown, yielding 30 mJy/rt(s), consistent with the predicted noise under 70% sky transmission conditions (Figure 11). These observations were obtained in the same night as the data of J1148+5251 were taken, when clouds were present all night. Note that a point source sensitivity of 30mJy/rt(s) in *time stream* data corresponds to a *map* point source sensitivity of 42 mJy/rt(Hz) for our 0.9 λ/D sampled pixels. Figure 12 shows the expected time sequence NEFD for GISMO with the 40% transmission neutral density filter. Figure 13 shows a histogram of the noise derived from 32 pixels during the same

observation shown in Fig. 11. Only pixels with response to the source about a given threshold (i.e. which were centrally crossed by the source) were selected; we found 32 such pixels, although the less-well-crossing pixels will bias the noise result upward. This selection results in an the apparent higher sensitivity of time stream data than what is seen in maps. The centroid of the histogram is at 35mJy/sqrt(s).

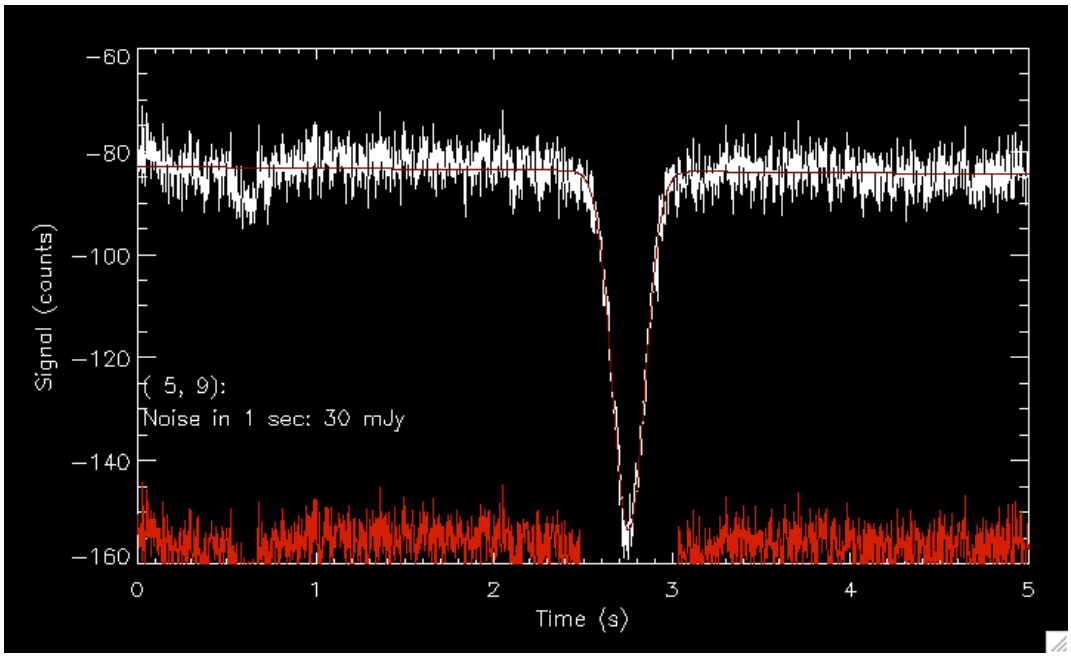

Figure 11: Time sequence showing the readout from a single pixel during a scan on 3C454.

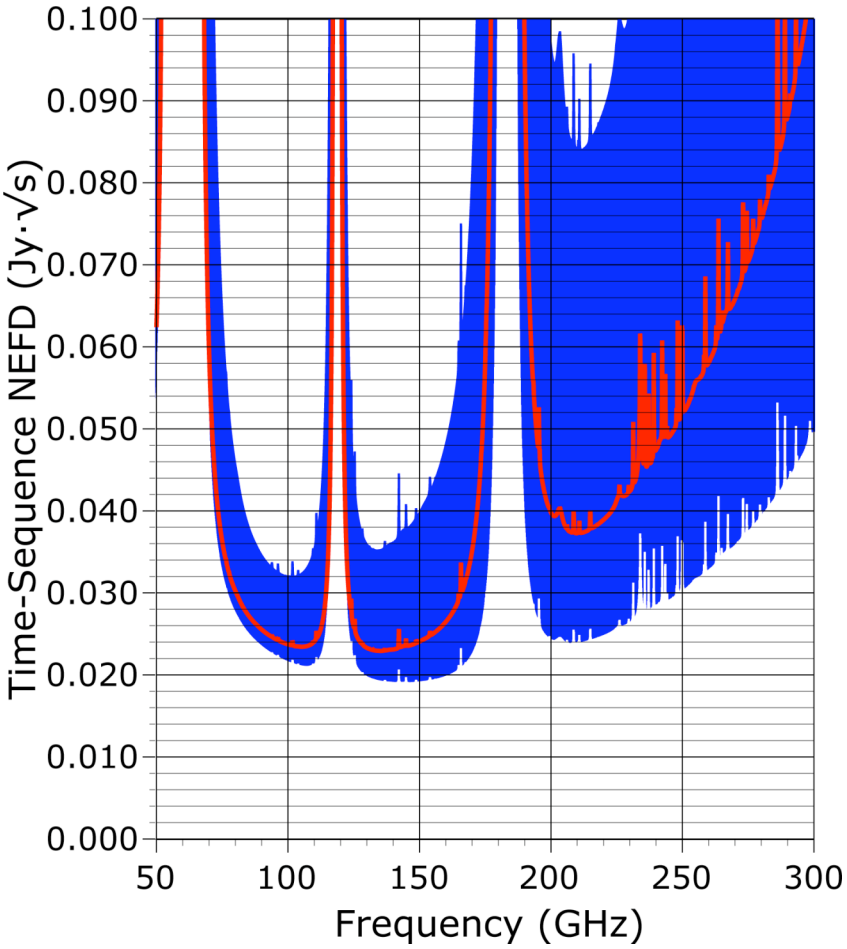

Figure 12 shows the expected NEFD for the time series data of "full" pixel crossings. It is the similar to the NEFD shown in Figure 9, but degraded due to the fact that the equivalent number of pixels illuminated by the source in the time stream is 2.06, whereas it is 4.07 pixels in our maps (the pixel size is 14", the HPBW of the telescope beam is 16").

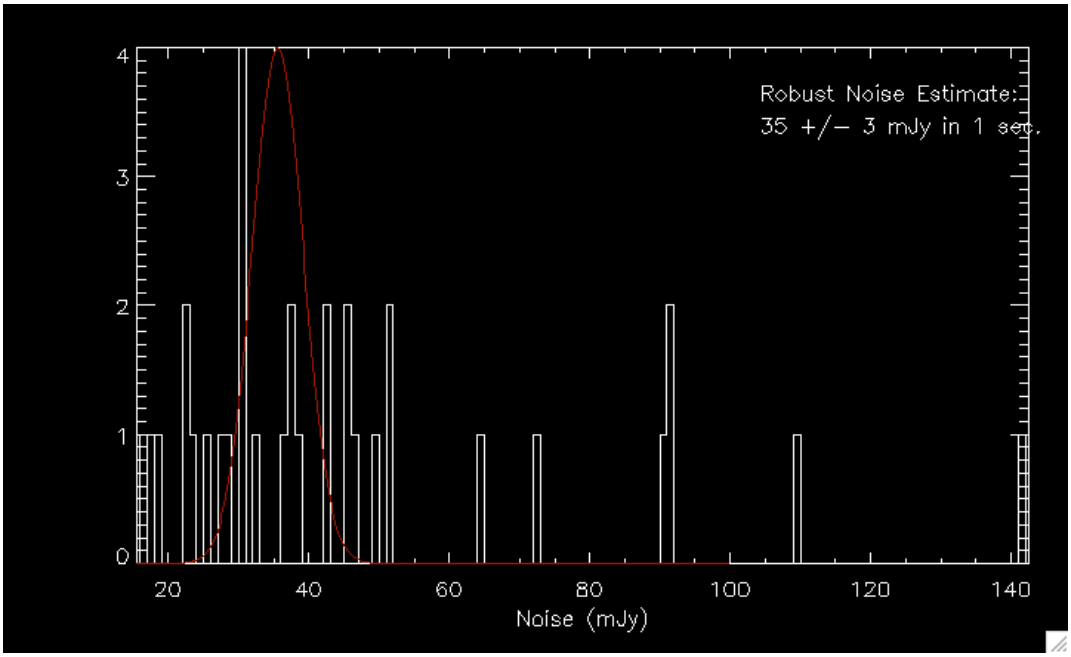

Figure 13: Histogram showing the noise derived from 32 pixels during the same observation shown in Figure 10. Only the 32 pixels with response to the source about a given threshold (i.e. which were centrally crossed by the source) were selected. The centroid of the histogram is at 35mJy/sqrt(s).

Data reduction with Crush-2: Recently Attila Kovacs ran a few of our GISMO data through his latest version of Crush-2, which allows data reduction of bolometer based cameras other than SHARC 2. A first look at the reduced data is very promising, in particular problems with negative emission around strong sources do not seem to occur. The achieved s/n (see discussion above) is similar to the results we obtain with our data reduction package. We have now a preliminary version of Crush-2 at hand and we will continue to compare its performance with that of our data reduction package. Figures 14 and 15 show results from GISMO Orion and 3C434 data, reduced with Crush-2.

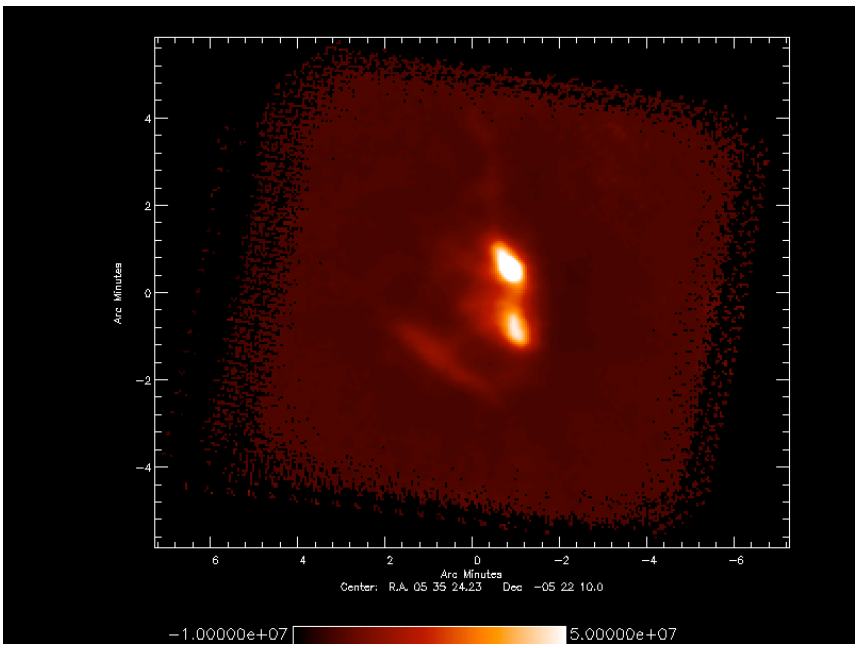

Fig. 13. A single scan of Orion, highpass filtered and run through Crush-2.

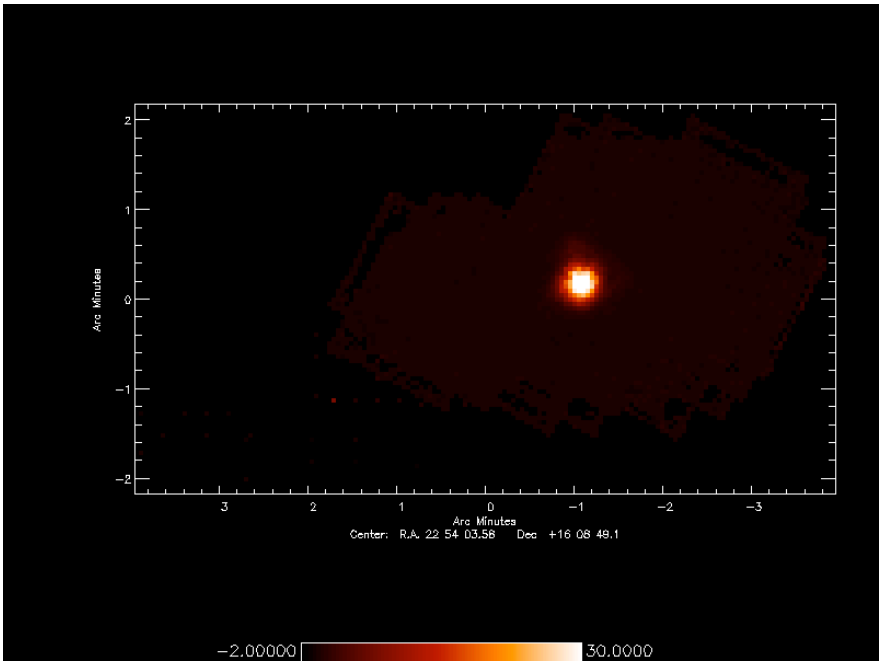

Fig. 14. GISMO raw data of 3C454 reduced with Crush-2.

Magnetic fields:

While redesigning the detector package, we were able to benefit from improved SQUID multiplexer designs which feature a reduced sensitivity to the magnetic fields. Additionally, we improved the magnetic shielding of the SQUIDs with the new readout mounting we developed. While GISMO was very sensitive to the Earth's field during run #1, we expected a greatly improved situation for run #2.

We swept the telescope around 12 degrees near Az=125°, recording three-axis magnetic fields with the GISMO window shutter blanked. The resultant pickup of the Earth's magnetic field is easy to see in the attached sample of five channels, shown in Fig. 15, although this is somewhat hysteretic due to instrument drifts during the 10 minute scan. After comparing all detectors and selecting those with the cleanest signal, a net pickup of 95.5 counts per microTesla is seen. No pickup significantly in excess of this is present in any valid channel. We convert this to an approximate pickup during scanning of around 0.3 counts per arcminute of azimuthal slew. Typical GISMO scans move only 2 arcminutes, and so the total effect of magnetic field pickup at this azimuth should be around 0.6 counts. This can be contrasted with typical sky noise variations of hundreds of counts during a typical scan. At this level, magnetic field pickup will be subsumed in the overall atmosphere model.

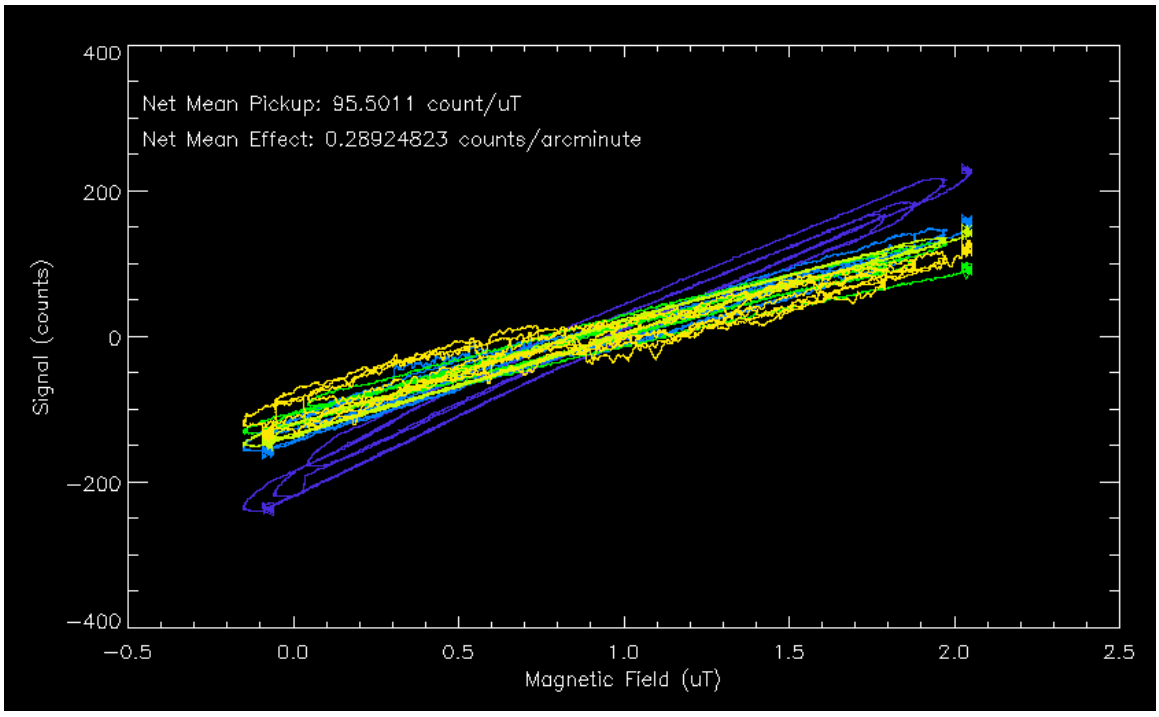

Figure 15: Recording of three-axis magnetic field measurements when the telescope was swept around 12 degrees near AZ=125. The detected signal from the GISMO detectors is displayed vs. the measured change in the magnetic field.

Internal calibration source

GISMO has an internal calibration source, consisting of an encased LED with fiber optic that (is supposed to) point towards the detector array. We have electronics that pulse the LED rapidly for lock-in detection. Due to a misalignment of the fiber optic we did not achieve the required illumination for sufficient signal strengths. The power required for a sufficient illumination of our pixels resulted in too much radiative heat from the LED to use it in routine mode. This can and will be easily fixed in the future.

Additionally, GISMO has a computer-controlled shutter in front of the instrument window. Due to problems with the digital electronics on the commercial controller board we used, we had difficulty controlling the shutter reliably. We have purchased a controller board from a different vendor with better heritage for use in future observing runs.

Major Post Observing Efforts

Detector package fixes: We fixed the two major problems that we had encountered during observing run # 2:
We replaced a SQUID multiplexer chip that had an internal short, which caused a crosstalk of the first stage SQUID feedback of column 1 into the second stage feedback of columns 2 & 3. We also replaced the connectors on the detector readout board, since the connectors we had used during the run created an address line crosstalk, that would not result in problems with the SQUID addressing, but was likely causing a ground loop situation which resulted in some of the channels showing increased noise and an apparent lower saturation power. After those two fixes we observe a positive effect in terms of the detector stability, we see virtually no unstable pixels in the lab (Fig. 16 shows a representative noise spectrum).

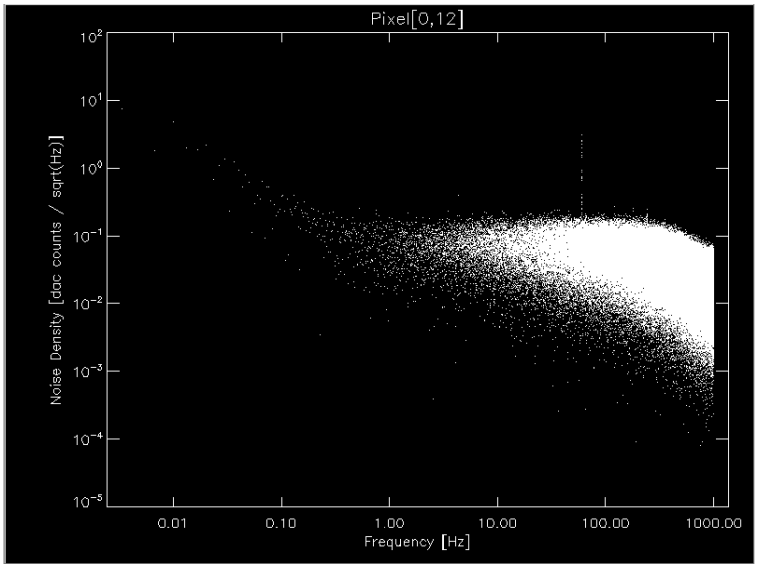

Figure 16: Typical Laboratory noise spectrum of a biased TES. We observe virtually no pixels that show excess noise.

Design of alternative neutral density filters: We have designed the required optical setup for a room temperature neutral density filter, which is based on the use of a polarizing grid and a, elliptical mirror. This setup will allow us to use GISMO without the cold 40% transmission filter during good to normal weather conditions without an instrument warmup.
At the same time we are exploring a cryogenic neutral density filter design that allows mving the filter in and out of the beam in front of the detector package.

New position for GISMO in the receiver cabin:
Our optical engineer is working together with IRAM on an optical setup that will provide a dedicated place for GISMO in the receiver cabin without the requirement to remove MAMBO from the receiver cabin during observations with GISMO.

Software tool improvements:

1) Data reduction: A large amount of efforts has gone into our data reduction algorithms and tools. In particular did we improve our algorithms for weak source observations. Three major improvements are: a) better identification of bad pixels, b) subtraction of several principal component vectors, which allows to subtract column specific features, c) Lissajous frequency filtering.
2) Data acquisition software: We have implemented automated IV curve measurements which allow total power measurements for calibration and bias setting adjustments and possibly trigger of neutral density filter use.

Conclusion

The following improvements of GISMO during run #2 as compared to run #1 were obtained:

- We observed a significant decrease in pickup noise in our data, resulting in much lower noise floor for the instrument.
- Stray beam (hot spillover) is eliminated, and so we have a greater saturation power range and better optical performance.
- Blackening of many cold components, including the inside of detector package lid, additionally reduces load on detectors and improves stray light response.
- Opto-isolators for all external signals allow for only one ground reference for the dewar and all electrical signals entering and exiting the dewar. The resulting improvements are demonstrated in Figure 1.
- Greatly enhanced tunability of SQUIDs and detectors, resulting in more optimal instrument performance during observing. The tuning processes are significantly more automated than before, making the user interface to GISMO more accessible to the novice.
- Greatly reduced magnetic field pickup, essentially eliminating this as a source of concern. This was achieved by oversizing the niobium foil under the SQUID multiplexer chips.

- Improved mapping efficiency using the IRAM Lissajous scan pattern, which was implemented specially for GISMO.
- Greater data processing automation through a standard pipeline that is run automatically via triggering from the IRAM messaging system.

The results from this observing run include:

- A demonstration that GISMO's achieved a sensitivities clodeley travce the predicted values. Due to the use of the neutral density filter the detector NEP was similar to the NEP during better weather conditions. Our simulations predict that removing the neutral density filter will result in very nearly sky photon-noise-limited performance under practically all weather conditions, with increased sensitivity.
- Noise integrates down radiometrically over thousands of observing seconds.
- High-quality images of extended sources, including Cas A, and the infrared cloud IRDC 30, where dust emission down to a level of 10 mJy was detected. .
- Numerous quasars and stars as system characterization.
- The derived instrument performance is independent of the method (sky map noise vs. time stream analysis) used to determine the point source signal-to-noise ratio for astronomical observations with GISMO. The results are consistent with our models; therefore we conclude that the instrument performance is well understood.